Available online at www.sciencedirect.com
SCIENCE DIRECT®
Journal of Power Sources 139 (2005) 371–378
JOURNAL OF POWER SOURCES
www.elsevier.com/locate/jpowsour

Influence of carbon nanotubes addition on carbon–carbon supercapacitor performances in organic electrolyte

C. Portet, P.L. Taberna, P. Simon*, E. Flahaut

CIRIMAT, UMR CNRS 5085, 118 Route de Narbonne, Toulouse, Cedex 31062, France

Received 29 April 2004; received in revised form 8 July 2004; accepted 10 July 2004
Available online 18 September 2004

Abstract

This paper presents the performances of 4 cm^2 supercapacitors cells assembled with 200 μm thick active material films composed with activated carbon and carbon nanotubes mixture in organic electrolyte. Galvanostatic and electrochemical spectroscopy impedance measurements have been carried out. Galvanostatic measurements show that both internal resistance and specific capacitance decrease when the carbon nanotubes content increases in the active material. With 15% of carbon nanotubes, the internal resistance is 0.65 Ω cm^2 and the specific capacitance is 90 F g^{-1} measured at 20 mA cm^{-2}. This performances remain stable during 10,000 cycles.

The characterization of the frequency behavior was made by Electrochemical Impedance Spectroscopy. For 15% of CNTs content in the active material, the relaxation time ($\varphi = -45°$) is divided by 3 as compared to a supercapacitor using pure activated carbon electrodes.

Keywords: Supercapacitor; Activated carbon; Carbon nanotubes; Power device

1. Introduction

Supercapacitors are electrochemical storage devices able to fill the gap existing between batteries and dielectric capacitors from the energy and power density point of view. As compared to batteries, supercapacitors can deliver higher power for shorter time; as compared to capacitors, they store higher energy but deliver lower power. These performances make them already useful in power electronics. They are now planned to be used in hybrid electrical vehicle (HEV), mainly for braking energy recovery and boost [1].

Three main types of supercapacitors are commonly described in the literature, depending on the electrode active material used: activated carbon [2,3], metal oxide [4,5] and electronically conducting polymer [6,7]. Supercapacitors based on metal oxide can deliver high power, but their cost limits their use to military or space applications. electronically conducting polymer-based supercapacitors are now still at the research state. Beside these three main technologies, hybrid supercapacitors have been recently developed using an activated carbon electrode with an electronically conducting polymer electrode [8,9].

Activated carbon-based supercapacitors are the most developed technology because of their low cost, large capacitance and long cycling life. Electrostatic charges are stored at the activated carbon/electrolyte double layer interface; there is no faradic reactions.

Carbon nanotubes (CNTs) are carbonaceous materials with particular properties: increased accessible surface area, low mass density and high electronic conductivity. These materials have then been studied by several authors in supercapacitor applications, mainly in aqueous electrolytes [10–14]. However, the specific capacitance of as-received CNTs remains lower compared to activated carbon. This explains why several treatment have been proposed to increase their specific capacitance such as polymer deposition [15,16] or physical/chemical activation [17,18].

Another way to take benefit from the electrochemical and electrical CNTs properties in supercapacitors applica-

* Corresponding author. Tel.: +33 5 61 55 68 02; fax: +33 5 61 55 61 63.
E-mail address: simon@chimie.ups-tlse.fr (P. Simon).

0378-7753/$ – see front matter © 2004 Elsevier B.V. All rights reserved.
doi:10.1016/j.jpowsour.2004.07.015

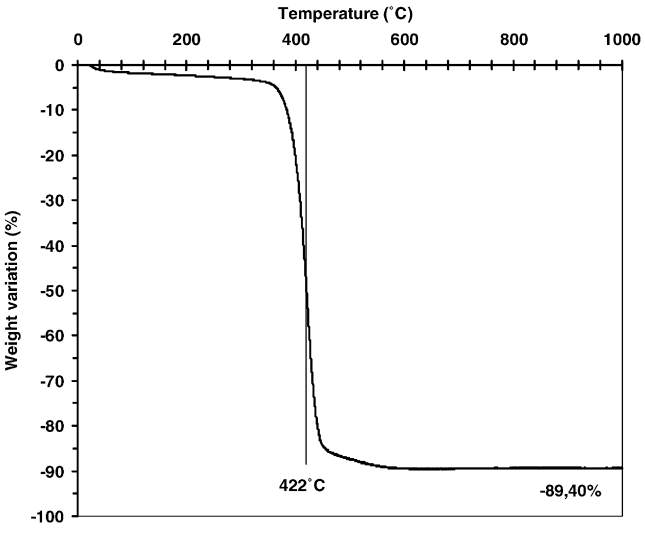

Fig. 1. TGA analysis of the DWNTs after catalyst elimination (1 °C min^{-1} in flowing air).

tion consists in adding CNTs to the activated carbon-base active material; which is the aim of this paper.

In this paper, we present the performances of carbon/carbon supercapacitors assembled with double-walled carbon nanotubes (DWNTs) [19,20] and activated carbon mixtures-based electrodes, in organic electrolyte. DWNTs are particular Multi-Wall CNTs (MWCNTs) since they have the smaller number of concentric walls. For this reason one can expect DWNTs to exhibit an intermediate behavior between SWNTs and MWNTs with number of walls higher than 2, limiting then the weight increase at the same specific capacitance.

The first part of this work presents the change of the cell parameters (ESR, capacitance) deduced from galvanostatic charge-discharge cycling experiments with respect to the CNTs content in the active material; this method allows the calculation of the average capacitance in the working potential window (from 2.3 down to 0 V) according to Eq. 1 (see below). The equivalent series resistance (ESR) was measured during a 1 ms current pulse; the corresponding potential was recorded and the ratio gives the ESR. This method also enables to characterize the aging of the cells during cycling.

In the second part, supercapacitors were studied by electrochemical impedance spectroscopy (EIS) in order to characterize the influence of the CNTs content on the frequency response of the cells. All the measurements are performed at OCV (fully discharge cell). The ESR measured at 1 kHz with EIS corresponds to the one obtained at 2.3 V in galvanostatic result.

2. Experimental

2.1. Synthesis of carbon nanotubes

The DWNTs were synthesised by catalytic chemical vapour deposition (CCVD) of a mixture of CH_4 (18 mol%) in H_2 on a MgO-based catalyst, at a temperature of 1000 °C [20]. The main interest of MgO-based catalysts is to be easily removable after the CCVD step. The catalyst, which can be written as $Mg_{0.99}M_{0.01}O$ (where M is a combination of Co and Mo: $Co_{0.75}Mo_{0.25}$), is not a solid solution (traces of an unidentified MoO_y oxide were detected by X-ray diffraction). Experimental details about the preparation of the catalyst have been reported elsewhere [20]. Af-

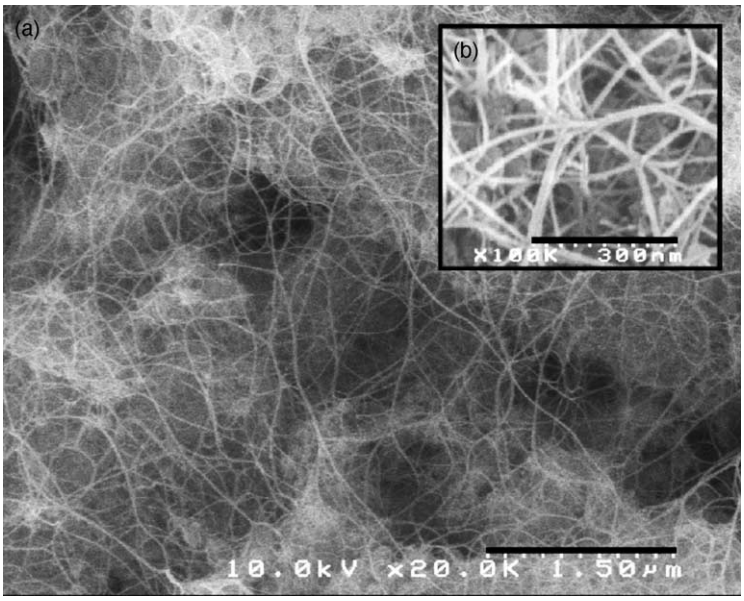

Fig. 2. (a) FEG-SEM image of the raw sample of DWNTs (before elimination of the catalyst), DWNTs after catalyst elimination (1 °C min^{-1} in flowing air). Inset (b) shows a higher magnification image of the bundles of DWNTs.

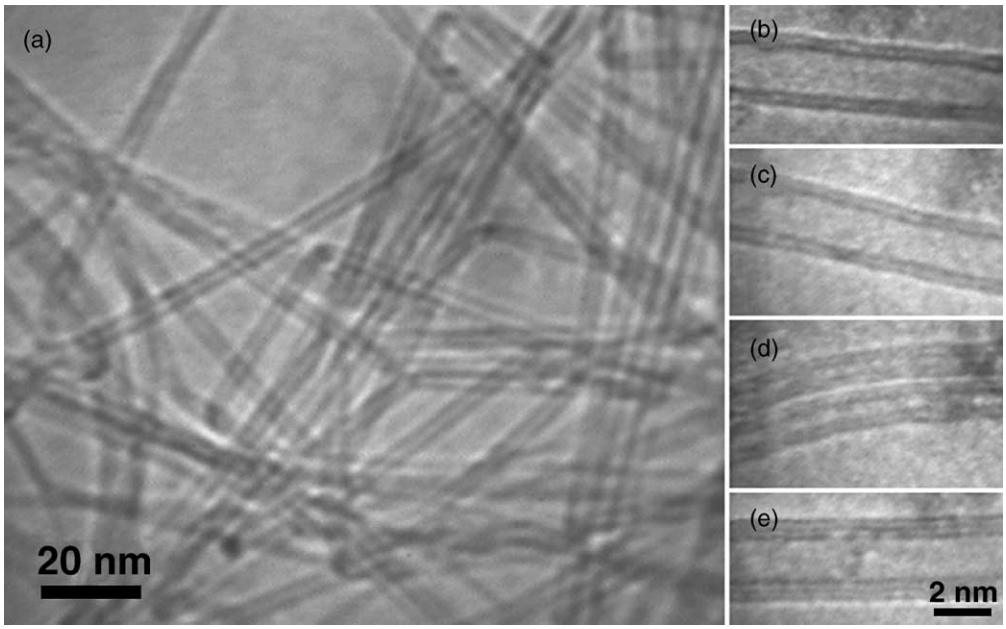

Fig. 3. (a) TEM image of the DWNTs sample; (b–d) high-resolution TEM images of DWNTs; (e) high-resolution TEM image of a triple-walled CNT.

ter the CCVD treatment, the so-obtained composite powder was reacted with concentrated aqueous HCl solution (overnight at room temperature) in order to remove the catalyst. The product was then washed with deionised water on a filtration membrane, until neutrality was reached. Drying was achieved in air, in an oven preheated at 80 °C. Thermogravimetric analysis [21a,b] (1 °C min^{-1} in flowing air, Fig. 1) shows only one well-defined weight loss at 420 °C, corresponding to 89.4% of the initial weight, in very good agreement with the elemental analysis (89.7 wt.% of carbon, measured by flash combustion). This corresponds to more than 97.7 mol% of carbon, assuming that the sample contains only cobalt and carbon. The BET specific surface area is around 985 m^2 g^{-1}. The remaining metal (2.3 mol%) is present in the sample as carbon-encapsulated nanoparticles. The metal is protected by the graphitic layers and thus not subject to oxidation or to interaction with its environment [22].

Fig. 2 shows a representative FEG-SEM image of the raw CNTs sample (before removal of the catalyst), revealing an important density of bundles of CNTs, with extensive branching. Their diameter is typically ranging between 10 and 20 nm. No carbon nanofiber could be observed in the sample. TEM observation (Fig. 3) was performed on the CNTs, after elimination of the catalyst. The CNTs are clean (no amorphous deposit) and generally isolated, or gathered into small-diameter bundles, mainly composed of DWNTs [23]. DWNTs represent more than 75% in number [20], according to the analysis of HRTEM images of isolated CNTs. The sample was analysed by Raman spectroscopy (Fig. 4). The Raman spectra of CNTs gives two kinds of information about the sample: (i) between 100 and 300 cm^{-1}, the radial breathing modes (RBM) are strongly depending on the diameter of the CNTs and models have been proposed to calculate the diameter from the frequency of the RBM peaks [24,25], the CNTs have diameters ranging from 1 (peak no 7, Fig. 4) to 2.2 nm (peak no l, Fig. 4), in good agreement with HRTEM observations (Fig. 3); (ii) at higher frequency (between 1250 and 1700 cm^{-1}), the Raman spectra is characterised by two main peaks centred at 1342 cm^{-1} (D peak) and 1588 cm^{-1} (G peak). The D peak is associated with crystalline disorder (sp-Mike carbon) and the G peak is associated with the $E2_g$ mode (stretching vibrations) in the basal-plane of graphite (sp^2 carbon). The ratio $I_{D/G}$ between the intensity of the D and the G peaks is often used to quantify the degree of crystallisation

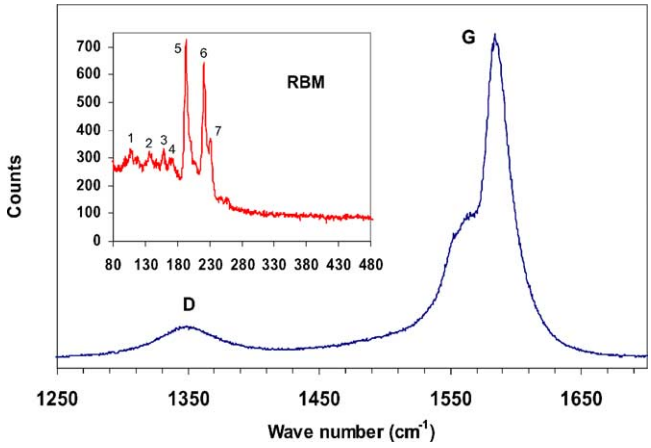

Fig. 4. Raman spectra of DWNTs. The ratio $I_{D/g}$ is around 9% The inset shows the RBM peaks and corresponds to CNTs with diameter ranging from 1 nm (peak no. 7) to 2.2 nm (peak no. l) (these values correspond to the average between the diameters calculated taking or not into account the bundling effect; the bundling typically shifts down the frequency by 4%).

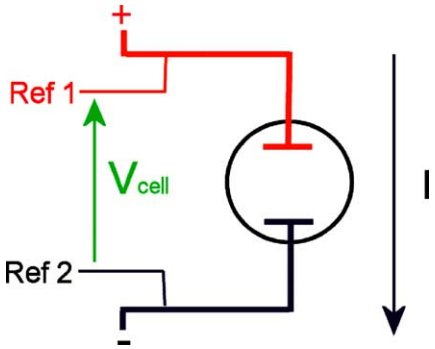

Fig. 5. Sketch of the measurement device.

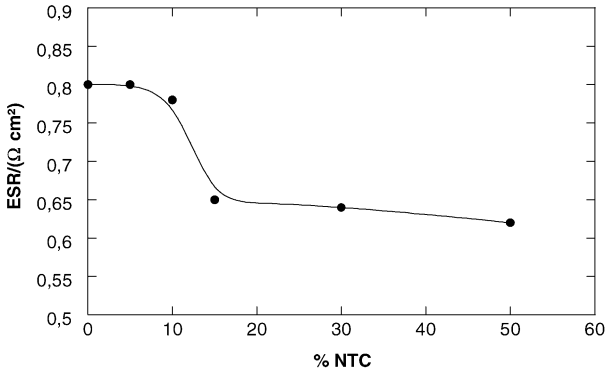

Fig. 6. Change of the ESR of 4 cm^2 supercapacitor assembled with various CNTs content in the active material.

of the samples of CNTs, low values of $I_{D/G}$ corresponding to a better crystallisation. The experimental value of $I_{D/G}$ is close to 9%, which corresponds to a good structural quality of the sample.

2.2. Constitution of carbon/carbon supercapacitor

A 4 cm^2 electrodes were made by laminating active material onto treated-Al current collector foil (200 μm thick). The current collector treatment consists in a conducting paint; the process has been described in a previous paper [26]. Carboxymethylcellulose (CMC, from Prolabo) and polytetrafluoroethylene (PTFE, from Dupont de Nemours) were used as binders. The active layer composition is *x* wt.% activated carbon, *y* wt.% CNT, 3% CMC and 2% PTFE, with $x + y = 95$. Activated carbon used is the PicactifBPIO from the Pica Company (Vierzon, France). Different active material composition were studied, varies from 0 to 50% CNTs content in the active material. The electrode thickness was kept constant at 200 μm.

Supercapacitor cells were assembled with 4 cm^2 electrodes between two PTFE plates in a glove box where water and oxygen are controlled (less than 1 ppm). The two electrodes were separated with a 50 μm thick porous polymeric film separator. Stainless steel clamps were used in order to maintain the stack under pressure. The organic electrolyte was 1.5 M NEttBF4 in acetonitrile, with water content lower than 10 ppm [27].

2.3. Electrochemical apparatus

Electrochemical characterizations were carried out using galvanostatic cycling and electrochemical impedance spectroscopy. The galvanostatic cycling was performed with a BT2000 Arbin cycler at different current densities from 5 mA cm^{-2} to 100 mA cm^{-2} between 0 and 2.3 V. A sketch of our measurement device is given on Fig. 5.

Electrochemical Impedance Spectroscopy measurements were made with an EGG 6310 apparatus between 10 mHz and 50 kHz at OCV when the cell is fully discharged.

3. Results and discussion

3.1. Galvanostatic cycling results

Cycles were performed at ±20 mA cm^{-2} between 0 and 2.3 V. The equivalent series resistance was measured during a 1 ms current pulse; the corresponding potential was recorded and the ratio gives the ESR.

Fig. 6 presents the influence of CNTs content in the active material on the equivalent series resistance of the supercapacitor cells. The ESR of the reference cell using activated carbon active material (0% CNTs) is 0.8 Ω cm^2. For low CNTs content, i.e. 5% and 10%, there is no significant change of the ESR as compared to the reference cell. For 15% CNTs, a sharp decrease of ESR is observed down to 0.65 Ω cm^2. For higher CNTs content, i.e. 30% and 50%, it tends to be constant around 0.6 Ω cm^2.

The supercapacitor equivalent series resistance is the sum of various contributions such as: electrolyte resistance (in the porosity and in the separator), Al current collector intrinsic resistance (neglected), active material/electrolyte interface resistance, active material intrinsic resistance and contact between the particles. The modification of the resistance is due to the presence of the CNTs in the active material; CNTs have higher electronic conductivity than activated carbon [2,28]. The activated carbon conductivity varies from few tens of mS cm^{-1} to up to 100 mS cm^{-1} depending on the activated carbon nature [2]. As compared to the activated carbon, the CNTs conductivity varies from few S cm^{-1} up to 1000 S cm^{-1}, depending on the CNTs nature (SWNTs, MWNTs,. . .) [28]. In this paper, the measurement of the DWNTs conductivity gave results between 30 up to 1000 S cm^{-1} and is 100 times superior to the activated carbon one.

The value of 15% seems to be the percolation threshold for our system: CNTs enhance both ionic and electronic conductivity inside the porous structure.

Fig. 7 presents the change of the specific capacitance of the active material versus the CNTs weight content in the active material. The cell capacitance is deduced from the slope of

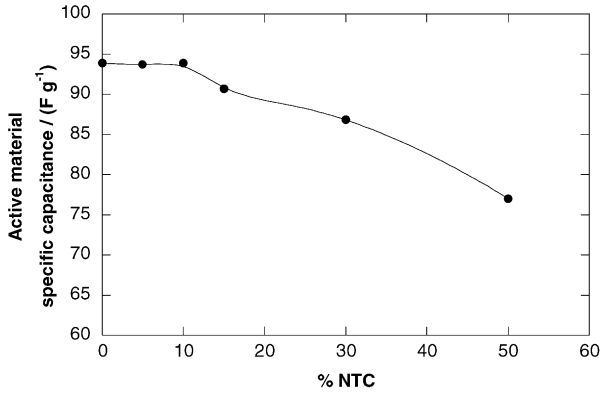

Fig. 7. Variation of the specific capacitance with different CNTs content in the active material between 0 and 2.3 V at a current density of 20 mA cm^{-2}.

the discharge curve with (1):

$$C = \frac{I}{(\mathrm{d}V/\mathrm{d}t)} \quad (1)$$

where C is the cell capacitance in Farad (F), I the discharge current in Ampere (A) and dV/dt the slope of the discharge curve in volts per second (V s^{-1}).

In a symmetrical system where the active material weight is the same for the two electrodes, the specific capacitance $C_{\mathrm{m_{AM}}}$ in farad per gram of active material (F g^{-1}) is related to the capacitance of the cell C by (2):

$$C_{\mathrm{m_{AM}}} = \frac{2C}{\mathrm{m_{AM}}} \quad (2)$$

where $\mathrm{m_{AM}}$ is the weight (g) per electrode of the active material.

Specific capacitance of the cell using activated carbon electrodes (0% CNTs) is about 95 F g^{-1}. With low CNTs content, i.e. 5–10 wt.%, it remains constant. When the CNTs content is increased up to 15%, the active material specific capacitance starts to decrease (90 F g^{-1}). For higher CNTs content, the more the CNTs content is increased, the less the specific capacitance (77 F g^{-1} at 50 wt.%). The specific surface area of CNTs is lower than that of the activated carbon; when the CNTs content increases, the specific surface area decreases as compared to activated carbon. CNTs probably gathered to form bundles, with only the outer surface accessible, creating then inter-tubes mesoporosity. When the CNTs content increases in the active material, there is a modification of the porous structure of the electrode.

Fig. 8 presents the change of the relative capacitance versus the cycling current density. Specific capacitance is maximum at low current density 5 mA cm^{-2}. When the current density is increased, the ohmic drop prevails the capacitance decreases for all the cells studied. The mass transfer kinetics, here the ionic migration, in the porous structure of the electrode becomes too low and limits the accessibility to the whole porosity, leading to the decrease of the capacitance as compared with low current density.

When the CNTs content is lower than 15%, there is a high dependence of the specific capacitance with the applied

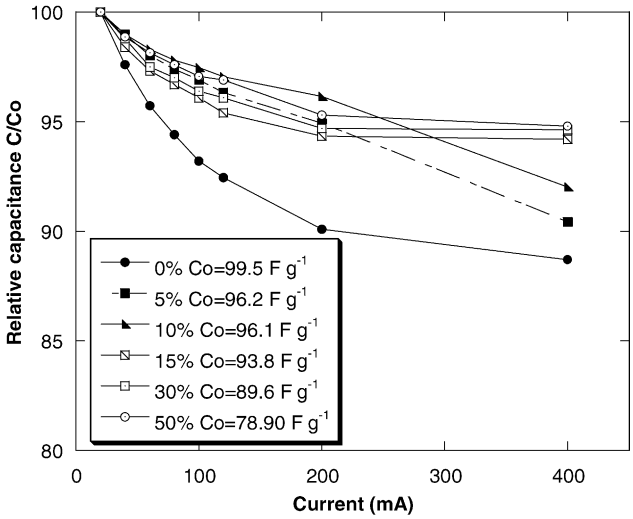

Fig. 8. Variation of the relative capacitance C/C_0 where C_0 represents the capacitance measured at 5 mA cm^{-2}.

current: the capacitance strongly decreases when the current density is increased. For CNTs content higher than 15%, the relative capacitance is less current dependent and the loss of capacitance becomes constant (around 6%) at high current density 100 mA cm^{-2}. From 5 to 100 mA cm^{-2}, the capacitance loss decreases when the CNTs content is increased. When the CNTs content increases, the pore size distribution is modified. The porous structure of the CNTs bundles develop less surface area (985 m^2 g^{-1}) as compared to an activated carbon (2300 m^2 g^{-1}) but the pore accessibility is higher with CNTs than activated carbon. When the current density is increased, the relative capacitance C/C_0 is stable with varying CNTs content as compared to activated carbon. CNTs are suitable to limit the capacitance loss when the current density increases.

A CNTs content of 15% seems to be a good compromise between stability and high specific capacitance.

A 4 cm^2 cell was assembled with electrodes containing 15 wt.% CNTs. Fig. 9 shows the change of the cell ESR during cycling between 0 and 2.3 V at a constant current of 100 mA cm^{-2}. The ESR was found to be stable around 0.65 Ω cm^2 on the whole cycling test (10,000 cycles); no faradic reactions occurred during cycling.

The active material composition that has been studied here leads to cell electrochemical characteristics interesting for supercapacitor applications: an ESR of 0.65 Ω cm^2 associated with a specific capacitance of 90 F g^{-1} of active material measured at 20 mA cm^{-2}.

3.2. Electrochemical impedance spectroscopy measurements

3.2.1. A 4 cm^2 cell with activated carbon-based electrodes

Fig. 10 presents the Nyquist plot of a 4 cm^2 cell supercapacitor between 10 mHz and 50 kHz at OCV. At higher fre-

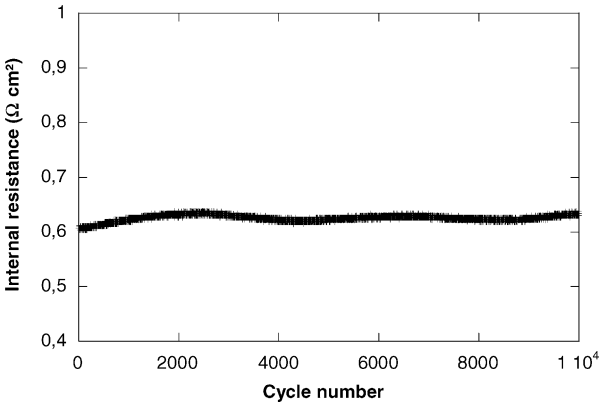

Fig. 9. Variation of the ESR of 4 cm^2 supercapacitor assembled with electrodes containing 15% of CNTs between 0 and 2.3 V at a constant current of 100 mA cm^{-2}.

quencies, the supercapacitor behaves like a pure resistance. When frequency is decreased, the ion migration inside the porous active material can be seen. At low frequencies, the imaginary part of the impedance increases, showing the capacitive behavior of the supercapacitor [29].

In a previous paper, we presented a simple way to modelize the supercapacitor frequency behavior by using the impedance data Eq. (2) [27]:

$$Z(\omega) = \frac{1}{j\omega C(\omega)} \tag{3}$$

The impedance $Z(\omega)$ can be written under its complex form:

$$Z(\omega) = Z'(\omega) + jZ''(\omega) \tag{4}$$

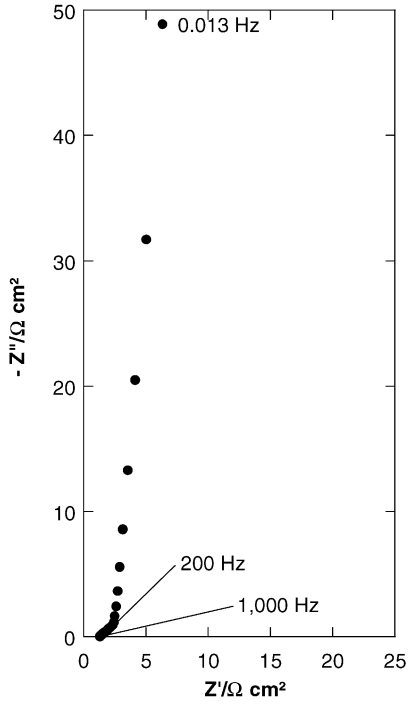

Fig. 10. Nyquist plot for 4 cm^2 cells assembled with electrodes constituted with activated carbon.

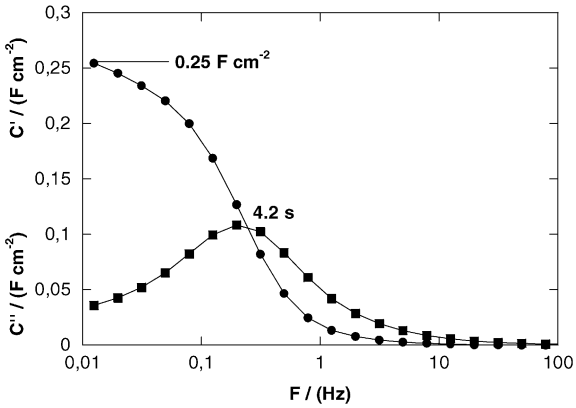

Fig. 11. Real and imaginary capacitance vs. frequency for 4 cm^2 supercapacitor cell assembled with electrodes constituted with activated carbon.

Eqs. (3) and (4) lead to Eq. (5)

$$C(\omega) = \frac{1}{\omega(jZ'(\omega) - Z''(\omega))} = \frac{-(Z''(\omega) + jZ'(\omega))}{\omega|Z(\omega)|^2} \tag{5}$$

It is then possible to define:

$$C(\omega) = C'(\omega) - jC''(\omega) \tag{5'}$$

leading to:

$$C''(\omega) = \frac{-Z''(\omega)}{\omega|Z(\omega)|^2} \tag{6}$$

$$C''(\omega) = \frac{Z'(\omega)}{\omega|Z(\omega)|^2} \tag{7}$$

where

- $C'(\omega)$ is the real part of the capacitance $C(\omega)$; the low frequency value of $C'(\omega)$ corresponds to the capacitance of the cell that is measured during constant current discharge, for example.
- $C''(\omega)$ is the imaginary part of the capacitance $C(\omega)$. It corresponds to an energy dissipation by some kind of irreversible processes that can take place and lead to a hysteresis, such as an example the dielectric losses in water occurring during the rotation or the movement of the molecules [27].

Fig. 11 presents the variation of the real part of the capacitance C with the frequency. At low frequency, the total capacitance of the electrode has been reached capacitance (IF); this low-frequency capacitance C_{LF} corresponds to the cell capacitance measured during galvanostatic cycling at ± 5 mA cm^{-2}. When the frequency is increased, the capacitance decreases and at high frequency the supercapacitor behaves like a pure resistance.

The change of C' with the frequency depends on many parameters, such as for example the nature of the electrolyte, the electrode thickness and the porous structure of the electrode.

Fig. 11 also presents the imaginary part of the capacitance C'' change with the frequency. C'' corresponds to the supercapacitor energy dissipation. C'' passes through a maximum

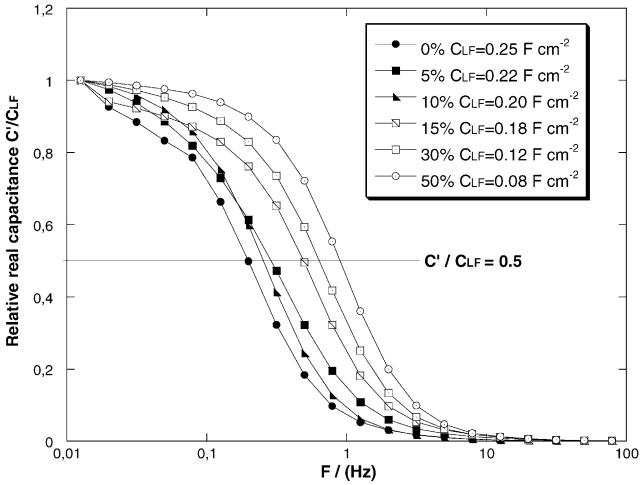

Fig. 12. Evolution of the real capacitance vs. frequency for 4 cm^2 supercapacitor cell assembled with different CNTs content in the active material.

at 200 mHz. From Fig. 11, it is possible to deduce the relaxation time constant that defines the frontier between the capacitive behavior ($C'' > C_{LF}/2$) and the resistive behavior ($C' < C_{LF}/2$) of the supercapacitor. The relaxation time is deduced from the frequency f_0 with $\tau_0 = 1/f_0$, f_0 can be obtained from the real capacitance plot at $C' = C_{LF}/2$ and from the imaginary capacitance plot where it corresponds to the peak frequency (Fig. 11). The reference cell has a relaxation time constant of 4.2 s.

3.2.2. A 4 cm^2 cell assembled with CNTs/activated carbon-based electrodes

Fig. 12 presents the change of the relative capacitance C'/C_{LF} with the frequency for different CNTs content in the active material. The highest low-frequency capacitance C_{LF} is obtained when using pure activated carbon-based electrodes, according to the results previously found. The important point is that higher relative capacitance is obtained at the same frequencies when the CNTs content in the active material is increased. When the CNTs content in the active material is increased, the whole capacitance is reached at higher frequency.

Some authors studied the influence of the active material thickness on activated carbon based-supercapacitor frequency behavior [30–32] by electrochemical impedance spectroscopy (EIS) investigations; Kotz and Carlen described theoretically the influence of the electrode thickness on the cell capacitance. When the electrode thickness is decreased, the cell capacitance decreases and higher capacitance is obtained at higher frequency. They explain this result by a modification of the electrode porous structure [30]. Du Pasquier et al. noticed a decrease in the cell capacitance with the electrode thickness and they attributed this result to the decrease in the electrode mass. For thin electrodes, the migration path in the electrode is smaller and the active material porosity is reached for higher frequency [31].

Ch. Emmenegger et al. studied the effect of MWCNTs on the supercapacitor performances. They observed that the specific capacitance decreases linearly with the electrode thickness and the electrode density; moreover, they noticed that the accessible volume is linked to the thickness and the mass density [32].

In this paper, the electrode thickness remains the same (200 μm). As C' depends on the electrode structure, the supercapacitor frequency behavior was attributed to a modification of the active material porosity. At high frequency and for high CNTs content, the signal penetrates deeply inside the porous structure and reaches the whole porosity. Moreover, the CNTs bundle porosity is more accessible to the ions of the electrolyte as it is manly in the mesoporous domain; the migration path is smaller compared to the one of the activated carbon pore. The porosity is reached at higher frequency as it is the case with a thin electrode.

The influence of the CNT content on the imaginary part of the capacitance C'' with the frequency can be seen in Fig. 13. Compared to the reference cell, the energy dissipation is divided by a factor of 1.5 for 15% CNTs and by 3 for 50% CNTs: CNTs use limits the energy loss. C'' becomes smaller when the CNTs content increases in the active material. The high pore accessibility explains the decrease in C''.

The time constant corresponding to the relaxation time deduced from Figs. 12 and 13 decreases when the CNTs content is increased. When compared to the reference cell using pure activated carbon electrodes, the relaxation time constant is divided by a factor of 2.5 for 15% CNTs and by 5 for 50% CNTs.

This results show that the resistive behavior is frequency-delayed and the capacitive behavior appears at higher frequencies.

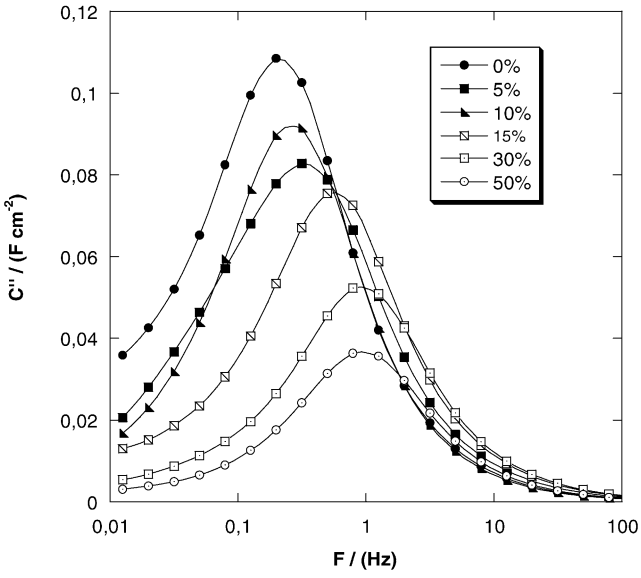

Fig. 13. Evolution of the imaginary capacitance vs. frequency for 4 cm^2 supercapacitor cell assembled with electrodes containing different CNTs content in the active material.

This result show that supercapacitor using activated carbon and CNTs content higher than 15% are suitable to deliver high power for short times.

4. Conclusions

This paper presents the performances of 4 cm^2 cell supercapacitor assembled with electrodes containing activated carbon and Carbon NanoTubes (CNTs) with different compositions. Seventy-five percent of the CNTs were double-walled carbon nanotubes.

Firstly, supercapacitors using activated carbon and CNTs have been studied by galvanostatic cycling measurements. For low CNTs content (5% and 10%), there was no changes on both internal resistance and cell capacitance as compared to a supercapacitor using activated carbon based electrodes. For CNTs content higher than 15%, the ESR is largely decreased leading to improved power performances for the cells. This was explained by a modification of the porous structure of the electrode. However, at the same time, an important specific capacitance decrease is observed. A CNTs content of 15% in the electrode has led to the best compromise in terms of specific power and energy performances.

Secondly, electrochemical impedance spectroscopy was used to characterize the cell frequency behavior, using the complex capacitance model. Results clearly showed that CNTs improved the cell performances. Here again, the best results were obtained with a CNTs content of 15% in the electrode: the characteristic frequency $f_0 = 1/\tau_0$, also called factor of merit, where half of the whole capacitance is reached, is around three times as much as the one obtained when pure activated carbon is used. A supercapacitor cell assembled with electrodes containing 15 wt.% of CNTs with activated carbon has led to the best results in terms of specific power and energy, with an equivalent series resistance of 0.65 $\Omega\,cm^2$, a specific capacitance of 90 $F\,g^{-1}$ of active material and a relaxation time of 1.6 s.

Acknowledgments

The authors want to thank the “Delegation Generate pour r 1 Armement” for financial support of this work.

References

[1] A. Burke, J. Power Sources 91 (2000) 37–50.
[2] J. Gamby, P.L. Taberna, P. Simon, J.F. Fauvarque, M. Chesneau, J. Power Sources 101 (2001) 109–116.
[3] T. Morimoto, K. Hiratsuka, Y. Sanada, K. Kurihara, J. Power Sources 60 (1996) 239–247.
[4] S.H. Pang, M.A. Anderson, T.W. Chapman, J. Electrochem. Soc. 147 (2000) 444–450.
[5] Q.L. Fary, D.A. Evans, S.L. Robertson, J.P. Zeng, J. Electrochem. Soc. 148 (2001) A833–A837.
[6] W.-C. Chen, T.-C. Wen, H. Teng, Electrochem. Acta 48 (2003) 641–649.
[7] M. Mastragostino, C. Arbizzani, F. Soavi, Solid State Ionics 148 (2002) 493–498.
[8] A. Du Pasquier, I. Plitz, S. Menocal, G. Amatucci, J. Power Sources 115 (2003) 171–178.
[9] A. Laforgue, P. Simon, J.F. Fauvarque, M. Mastragostino, F. Soavi, J.F. Sarrau, P. Lailler, M. Conte, E. Rossi, S. Saguatti, J. Electrochem. Soc. 150 (2003) A645–A651.
[10] F. Frackowiak, K. Jurewicz, K. Szostak, S. Delpeux, F. Beguin, Fuel Process. Technol. 213 (2002) 77–78.
[11] B-J. Yoon, S-H. Jeong, K-H. Lee, H.S. Kim, C.G. Park, J.H. Han, Chem. Phys. Lett. 388 (2004) 170–174.
[12] A.K. Chatterjee, M. Sharon, R. Banerjee, M. Neumann-Spallart, Electrochem. Acta 48 (2003) 3439–3446.
[13] Ch. Emmenegger, P. Mauron, A. Zuttel, Ch. Niitzenadel, A. Schneuwly, R. Gallay, L. Schlapbach, Appl. Surf. Sci. 162–163 (2000) 452–456.
[14] J.H. Chen, W.Z. Li, D.Z. Wang, S.X. Yang, J.G. Wen, Z.F. Ren, Carbon 40 (2002) 1193–1197.
[15] K. Hyeok An, K.K. Jeon, J.K. Heo, S.C. Lim, D.J. Bae, J. Electrochem. Soc. 149 (2002) A1058–A1062.
[16] K. Jurewicz, S. Delpeux, V. Bertagna, F. B6quin, E. Frackowiack, Chem. Phys. Lett. 347 (2001) 36–40.
[17] Q. Jiang, M.Z. Qu, G.M. Zhou, B.L. Zhang, Z.L. Yu, Mater. Lett. 57 (2002) 988–991.
[18] R.Z. Ma, J. Liang, B.Q. Wie, B. Zhang, C.L. Xu, D.H. Wu, J. Power Sources 84 (1999) 126–129.
[19] E. Flahaut, A. Peigney, Ch. Laurent, A. Rousset, J. Mater. Chem. 10 (2000) 249–252.
[20] E. Flahaut, R. Bacsa, A. Peigney, Ch. Laurent, Chem. Commun. (2003) 1442–1443.
[21] (a) E. Flahaut, A. Peigney, Ch. Laurent, J. Nanosci. Nanotech. 3 (2003) 151–158;
(b) S. Gajewski, H.E. Maneck, U. Knoll, D. Neubert, I. Dorfel, R. Mach, B. Straufl, J.F. Friedrich, Diam. Relat. Mater. 12 (2003) 816–820.
[22] E. Flahaut, F. Agnoli, J. Sloan, C. O’Connor, M.L.H. Green, Chem. Mater. 14 (2002) 2553–2558.
[23] J.F. Colomer, L. Henrard, E. Flahaut, G. Van Tendeloo, A.A. Lucas, Ph. Lambin, Nano. Lett. 3 (5) (2003) 685–689.
[24] L. Alvarez, A. Righi, T. Guillard, S. Rols, E. Anglaret, D. Laplace, J.L. Sauvajol, Chem. Phys. Lett. 316 (2000) 186–192.
[25] S. Bandow, S. Asaka, Y. Saito, A.M. Rao, L. Grigoran, E. Richti, P.C. Eklund, Phys. Rev. Lett. 80 (1998) 3779–3782.
[26] P.L. Tabema, P. Simon, J.F. Fauvarque, J. Electrochem. Soc. 150 (3) (2003) A292–A300.
[27] C. Portet, P.L. Tabema, P. Simon, C. Laberty-Robert, Electrochem. Acta 49 (6) (2004) 905–912.
[28] J. Wei, H. Zhu, B. Jiang, L. Ci, D. Wu, Carbon 41 (2003) 2495–2500.
[29] R. De Levie, Electrochim. Acta 8 (1963) 751–780.
[30] R. Kotz, Carlen, Electrochim. Acta 45 (2000) 2483–2498.
[31] A. Du Pasquier, J. A. Shelburne, I. Plitz, F. Badway, A. S. Gozdz, G. G. Amatucci, in: Proceedings of the 11th International Seminar on Double-Layer Capacitors and Similar Energy Storage Devices, Deerfield Beach, FL, 3–5 December 2001.
[32] Ch. Emmenegger, Ph. Mauron, P. Sudan, P. Wenger, V. Hermann, R. Gallay, A. Ziittel, J. Power Sources 124 (2003) 321–329.